Molecular modelling and electrochemical evaluation of organic inhibitors in concrete

M.V. Diamanti[1,*], E.A. Pérez Rosales[2], G. Raffaini[1,*], F. Ganazzoli[1], A. Brenna[1], M. Pedeferri[1], M. Ormellese[1]

[1] *Department of Chemistry, Materials and Chemical Engineering "Giulio Natta", Politecnico di Milano, Via Mancinelli, 7 – 20131 Milan, Italy*

[2] *Santos Ltd, 60 Flinders Street – 5000 Adelaide, South Australia*

Corresponding Authors:

Maria Vittoria Diamanti

Department of Chemistry, Materials and Chemical Engineering ''G. Natta'', Politecnico di Milano

Address: Via Mancinelli 7, 20131 Milan, Italy

Phone no.: 0039 02 23993137

Fax no.: 0039 02 23993180

Email: mariavittoria.diamanti@polimi.it

Giuseppina Raffaini

Department of Chemistry, Materials and Chemical Engineering ''G. Natta'', Politecnico di Milano

Address: Via Mancinelli 7, 20131 Milan, Italy

Phone no.: 0039 02 23993068

Fax no.: 0039 02 23993180

Email: giuseppina.raffaini@polimi.it

Abstract

Although corrosion inhibitors are largely used to prevent chloride-induced corrosion in reinforced concrete structures, their interaction mechanisms with the passive film present on steel still requires deeper understanding. This work combines experimental techniques with theoretical calculations, based on molecular mechanics and molecular dynamics methods of the adsorbed inhibitors on γ-FeOOH, to provide insight into the interactions between five organic inhibitors and carbon steel in a chloride-rich alkaline environment. A strong physisorption of inhibitors on the substrate was observed, while the distribution of specific groups - carboxylate anions or amino groups - and interactions among inhibitor molecules determined through molecular simulations drive the corrosion inhibition efficiency of the adsorbed layer.

Keywords: (A) steel reinforced concrete; (B) EIS; (B) molecular dynamics simulations; (C) pitting corrosion; (C) passive films

1. Introduction

Corrosion of steel embedded in concrete is one of the major causes of degradation of concrete structures. Normally, steel reinforcements are in passive condition, promoted by the concrete alkalinity. However, the passive film may be destroyed and corrosion may occur, mainly by two specific conditions: a) carbonation of concrete, which is the reaction of atmospheric carbon dioxide with the cement paste; b) presence of chlorides at the carbon steel surface in a content higher than a critical value [1].

Prevention of corrosion is primarily achieved in the design phase by using high quality concrete, i.e., low water/cement ratio, curing as long as possible and adequate cover. Additional prevention methods, such as blended cements, corrosion inhibitors, external concrete coatings, corrosion resistant rebars, cathodic protection, are adopted in severe environmental conditions or on structures requiring very long service life [1].

Among these methods, corrosion inhibitors are very attractive due to their low cost and easy handling [2]. They can be added to the concrete mixture as liquid additives to prevent corrosion, or they can be applied on the hardened concrete surface, allowing them to migrate towards the reinforcement, to reduce corrosion rate or to delay initiation time. Nitrite-based compounds are the most effective corrosion inhibitors [3-5]. First studies on nitrite-based compounds date back to the late 1950s [4], while systematic investigations as additives to fresh concrete started in the 1960s. Commercial products are available since 1970. Due to its oxidizing properties, nitrite is a passivating inhibitor: its inhibitive effectiveness is related to the $[NO_2^-]/[Cl^-]$ molar ratio, that should be higher than 0.5-0.6 to prevent corrosion [3-5].Unfortunately, nitrite-based inhibitors present several drawbacks such as toxicity, mechanical losses and risky effects when added in poor dosage.

For this reason, in the last 30 years new organic and inorganic products have been studied: molibdates, borates and sodium mono-fluoro-phosphates [6-8]; mixtures of alkanolamines and amines; emulsions of unsaturated fatty acid esters of an aliphatic carboxylic acid and saturated fatty acids [9-21]. The first commercial organic inhibitors, based on a mixture of amines and alkanolamines, were used in the 1980s. But, as reported in the state of the art by Elsener [2], there is no agreement among the scientific community in defining the effectiveness of these inhibitors: conflicting results are reported [9-21], the chemical composition of the organic commercial inhibitors and the concentration of the inhibitive substances are unknown. So far, most research has been focalised on determining the efficiency of some new substances as corrosion inhibitors, both in solution and concrete.

To define the more efficient compound, the interaction mechanism between organic inhibitors and the carbon steel passive film has to be investigated [22-29]. The development of new organic corrosion inhibitors is based on compounds containing nitrogen, oxygen and sulphur atoms, in addition to multiple bonds in the molecule that facilitate their adsorption on the passive metal surface of the carbon steel rebar. The adsorption is favoured by the presence of specific functional groups: electron-donor substituents, that release electrons, promoting the adsorption through the negative charge localisation on oxygen and on carboxylic group; negatively charged substituents, able to develop a repulsive action towards chloride ions, avoiding chloride to be in contact with the carbon steel passive layer; alkyl chains or voluminous substituent groups, which form a physical barrier [2, 22, 25-29].

In a previous extended research [25] a series of 80 organic compounds were studied: based on electrochemical tests in chloride containing alkaline solutions, amines showed poor inhibition effect, aminoacids showed some inhibition effect, but not sufficient for an industrial applications, while carboxylate substances, especially poly-carboxylates, showed very good inhibition effectiveness [22, 25]. The most efficient substances, also compatible with the properties of fresh and hardened concrete, were sodium tartrate, sodium benzoate, sodium glutamate, dimethylethanolamine and triethylenetetramine.

In this work, potentiodynamic tests and electrochemical impedance spectroscopy were performed to study the adsorption of the previously identified inhibitors on passive carbon steel. In parallel, to understand the interaction between these organic inhibitors and the exposed passivating film, computer simulations based on Molecular Mechanics (MM) and Molecular Dynamics (MD) methods were used [30] to establish the interaction energy between the inhibitors and the surface, the functional groups involved in the interaction and the mobility of the adsorbed molecules. The passivity of the carbon steel rebar in concrete was simulated by adopting as adsorption substrate a lepidocrocite (γ-FeOOH) passive surface, as reported in reference works [31-35].

2. Experimental

The experimental section of the research focused on the analysis of the corrosion behaviour of carbon steel immersed in a simulated concrete pore solution. Chlorides were added to the electrolyte to initiate localised corrosion, while five organic inhibitors were employed to delay corrosion initiation and reduce corrosion rate. Organic substances used as inhibitors were: two carboxylate compounds, sodium tartrate (Ta) and sodium benzoate (Be); one long chain aminoacid, sodium glutamate (Glu); and two amines, dimethylethanolamine (DMEA) and triethylenetetramine (TETA). Commercial products with a high degree of purity, except for TETA (purity: 70%), were used. Table 1 contains a summary of all inhibitors considered.

Table 1 – Composition and labels of organic inhibitors tested

Inhibitor	*Molecular structure*	*Label*
Sodium tartrate	$^{-}OOC–(CHOH)_2–COO^{-}\ Na^{+}$	Ta
Sodium benzoate	$C_6H_5–COO^{-}\ Na^{+}$	Be
Sodium glutamate	$^{-}OOC–(CH_2)_2–CH(NH_2)–COO^{-}\ Na^{+}$	Glu
Dimethylethanolamine	$(CH_3)_2N–CH_2CH_2OH$	DMEA
Triethylenetetramine	$NH_2–CH_2CH_2–(NHCH_2CH_2)_2–NH_2$	TETA

2.1 Electrochemical characterization

2.1.1 Materials

Specimens were cut from commercial reinforcing carbon steel with 10 mm diameter. Specimens were sandblasted and covered with self-adhesive tape on both ends, in order to leave an exposed surface area of 18.8 cm^2 (60 mm length).

Electrochemical tests were performed in simulated concrete pore solution, consisting of saturated $Ca(OH)_2$ with the addition of 0.06 M NaOH to reach pH 13. When needed, chlorides were added in the form of 0.1 M or 0.3 M NaCl. Tests were performed at room temperature (~ 25ºC).

2.1.2 Electrochemical tests

The characterization relied on three techniques: potentiodynamic polarization, free corrosion tests and Electrochemical Impedance Spectroscopy (EIS). The instrumentation used was an Autolab Potentiostat PGSTAT 30. As reference electrode, a saturated calomel electrode (SCE, +244 mV with respect to the standard hydrogen electrode SHE) was used, while the counter electrode was a platinum wire.

Free corrosion tests were performed to establish time-to-pitting initiation as a function of chloride content and increasing inhibitor dosage, namely: 0.0001 M, 0.001 M, 0.01 M, 0.1 M and 0.3 M. Specimens were passivated in the simulated pore solution for 168 hours, during which the free corrosion potential was monitored daily. When passivation was reached (i.e., about 1 week), 0.1 M NaCl was added to the solution. Potential measurements continued until initiation of corrosion. Time-to-corrosion was detected when free corrosion potential decreased from values typical of passive conditions (approx. -0.1 V SCE) to values typical of active conditions (approx. -0.5 V SCE). For comparison, tests were performed in simulated pore solution without inhibitors: in this condition time-to-corrosion, estimated starting from chlorides addition, was 2 h.

Potentiodynamic tests were employed to determine pitting potential in simulated pore solution in presence of 0.1 M of inhibitor and 0.1 M, 0.3 M or 1 M NaCl. Potential scan was performed starting at -0.8 V SCE with scan rate 1 V/h until a current density of 10 A/m^2 was reached: then, the scan was reversed in cathodic direction until the initial value was reached. Pitting potential was evaluated as the potential corresponding to a sudden increase in anodic current density.

Electrochemical Impedance Spectroscopy (EIS) tests were used to determine the adsorption parameters of organic inhibitors. A specific sample preparation was used for EIS tests: specimens were embedded in epoxy resin, grinded with emery papers of decreasing particle size (from 120 to 1200), washed with distilled water and degreased with acetone: the resulting surface area exposed was approximately 0.5 cm^2. EIS impedance spectra were recorded after 48 hours of immersion of specimens in simulated pore solution. In order to see the evolution of the interaction between the inhibitors and the passive film, the samples were immersed in solutions with different concentrations of inhibitor (0.0001 M, 0.001 M, 0.01 M, 0.1 M). After the first measurement, 0.1 M NaCl was added to the solution and EIS measurements were repeated at fixed times until corrosion occurred. EIS spectra were obtained by first measuring the steel open circuit potential (E_{OCP}), then by externally applying this value potentiostatically for the whole duration of the EIS test, on which a perturbation of amplitude ±10 mV was applied; spectra were recorded in a frequency range 100 kHz to 5 mHz. EIS was performed under computer control using the FRA v4.8 software; data were analysed with the ZSimpWin v3.10 software.

2.2 Calculation of adsorption isotherms

The results of EIS and potentiodynamic polarization tests were further processed to investigate the adsorption behaviour of the substances tested, and in particular to calculate the isotherm adsorption parameters. In particular, two models were applied to have a better understanding of adsorption phenomena: the Temkin isotherm and the generalised Langmuir-Freundlich (LF) isotherm, which can describe both the Langmuir-type and Freundlich-type adsorption behaviour. In the Temkin isotherm, lateral interactions between adsorbed molecules and presence of surface heterogeneities are taken into account, while the generalised LF isotherm considers only the latter effect.

Assuming that the charge transfer resistance can be related to the corrosion rate by the Stern-Geary equation, the parameters estimated from EIS electrical model can be used to calculate the inhibitor fractional surface coverage, θ, as proportional to the inhibitor efficiency:

$$\theta = 1 - \frac{i_{inh}}{i_o} = 1 - \frac{R_{1,o}}{R_{1,inh}} \quad (1)$$

where i_0 and i_{inh} are the corrosion rate for freely corroding and inhibited systems, respectively; $R_{1,0}$ and $R_{1,inh}$ are charge transfer resistances for freely corroding and inhibited systems, respectively.

The θ values calculated in this way were fitted to different isotherms, obtaining the best results with the abovementioned Temkin and the generalised LF isotherms.

θ was then introduced in the Temkin isotherm equation as follows:

$$K_{ads}C = e^{f\theta} \quad (2)$$

where C is the adsorption concentration, K_{ads} is equilibrium constant for the adsorption reaction, and f is the molecular interaction constant. Similarly, θ was introduced in generalised LF isotherm equation:

$$K_{ads}C = \left(\frac{\theta}{1-\theta}\right)^{\frac{1}{h}} \quad (3)$$

where h is a heterogeneity parameter, as a measure of adsorption energy distribution on a non-ideal surface. This isotherm has been successfully used for determining the adsorption of different inhibitors on iron in active and passive state [36-39].

Figure 6 and Table 1 report the isotherm plots and adsorption parameters, respectively. As expected, the inhibitor fractional surface coverage increases with inhibitor concentration. The equilibrium constant for the adsorption reaction, K_{ads}, is related to the adsorption standard free energy, ΔG^{o}_{ads}, by the following relationship:

$$K_{ads} = \frac{1}{55.5} e^{\left(-\frac{\Delta G^{o}_{ads}}{RT}\right)} \quad (4)$$

where 55.5 corresponds to the concentration of water in moles per litre, R is the ideal gas constant and T the absolute temperature [37].

2.3 Molecular Mechanics and Molecular Dynamics simulation protocol

A simulation protocol developed to model surface physisorption [40,41] was adapted to study both the interaction energy between inhibitors and steel passive film and the conformational properties of the molecules adsorbed on the lepidocrocite (γ-FeOOH) surface, in particular the (010) crystallographic face, which exposes hydroxyl groups, having the size of 39.96 Å × 38.70 Å with the *b* axis perpendicular to the surface. At first the lowest energy conformation of the isolated inhibitor molecules of Table 1 was determined. In particular, for glutamate we considered the (*S*) enantiomer, the natural aminoacid, and for tartrate the (*R*,*S*) or *meso* compound. The single molecule was then placed close to the surface in two different starting geometries, namely parallel or perpendicular to the surface, and its energy was minimised. Finally, the inhibitor molecules were randomly placed close to the lepidocrocite surface so as to study the possible surface covering and the molecules mobility during the time evolution of the system at a constant (room) temperature. The Materials Studio Modelling v.3.2.0.0 software [35] was used, adopting the Condensed-phase Optimized Molecular Potentials for Atomistic Simulation Studies (COMPASS) force field,

distributed with the software. A force field gives the potential energy of the system as a function of the coordinates of all the constituent atoms, and can be expressed through appropriate bonded and non-bonded energy contributions. The former contributions account for bond stretching and bending and for the torsional potentials taking as a reference the ideal values shown by analogous atoms in model compounds. The non-bonded terms account for the Coulombic interactions involving integer or fractional charges (for the dipolar interactions) and for the dispersive and co-volume interactions through a Lennard-Jones – or similar – analytical function. The COMPASS parameters and the ideal values for individual atoms in their chemical environments were previously published and validated [42] and are included in the force field database. The solvent was modelled as a dielectric medium with a distance-dependent dielectric constant. Ensembles of 16, 25 and 36 molecules were initially considered, but only the largest one was then subjected to MD simulations to study the possible full coverage of the surface. Energy minimizations with respect to all variables (atomic coordinates) were performed with the conjugate gradient algorithm up to an energy gradient lower than 4×10^{-3} kJ mol^{-1} Å^{-1}. The MD runs were performed at a constant *T* (300 K) controlled through the Berendsen thermostat. Integration of the dynamical equations was carried out with the Verlet algorithm using a time step of 1 fs (10^{-15} s), and the instantaneous coordinates (or frames) were periodically saved for further analysis or geometry optimization. MD runs were carried out until equilibration, monitored through the time changes of the system energy and of its components: this required runs of 0.5 ns for the carboxylate inhibitors, while 0.25 ns were sufficient for the neutral molecules when the monolayer formation was modelled.

Concerning data analysis, the geometries periodically sampled in the MD runs were analysed through the pair distribution function PDF, which gives the probability density of finding a set of atoms *j* at a distance *r* from another set of atoms *i*, and is defined as

$$\mathrm{PDF} = \frac{\mathrm{d}\langle N_{ij}(r)\rangle}{\mathrm{d}V(r)} \qquad (5)$$

where $\mathrm{d}\langle N_{ij}(r)\rangle$ is the average number of times the *j* atoms are comprised in a spherical shell of thickness d*r* at a distance *r* from atoms *i* within an MD run. Thus, the PDF yields the average local density of atoms *j* (for instance, the carboxylate oxygens in the anionic inhibitors) in the shell volume d*V(r)* at a distance between *r* and *r*+d*r* from atoms *i* (the exposed surface OH groups), yielding an immediate description of the local density of *j* atoms. In this way, we can give a simple picture of the average distances between selected functional groups of the inhibitors and the exposed surface atoms.

3. Results and discussion

3.1 Potentiodynamic polarization

Potentiodynamic tests, as well as free corrosion tests, were performed in alkaline solutions containing the selected inhibitor and various contents of sodium chloride. To describe the behaviour observed, DMEA is chosen as example: Figure 1 reports the anodic potentiodynamic polarization of carbon steel in simulated pore solution with two concentrations of DMEA (0.1 M and 0.3 M) and different contents of chlorides. Curves are compared with analogous tests performed in absence of inhibitor. In all conditions tested, the changes in behaviour were related to a variation of pitting potential, while no effect was noticed on either corrosion potentials or corrosion current densities in the passive range. Moreover, no repassivation is observed: the same absence of repassivation and of effects on the corrosion current density was produced by all other tested inhibitors.

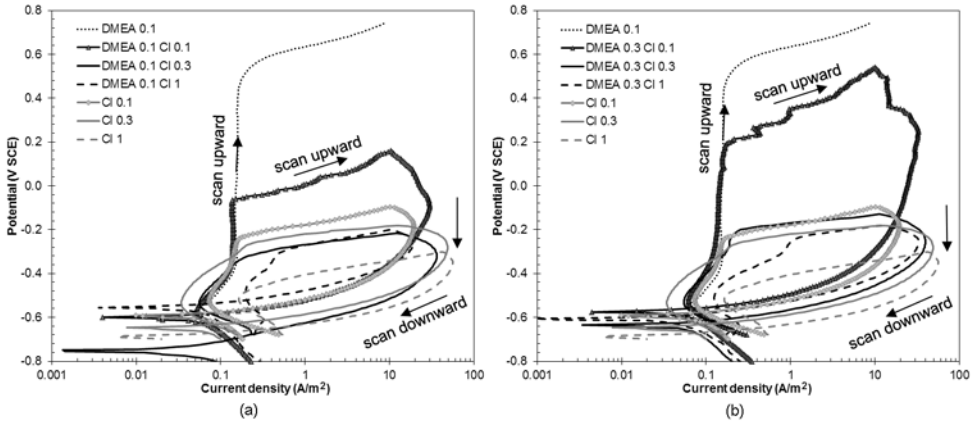

Figure 1 – Potentiodynamic tests on carbon steel in simulated pore solutions with the addition of 0.1 or 0.3 M DMEA and 0.1, 0.3 or 1 M NaCl

It is possible to observe how 0.1 M of DMEA is not sufficient to protect steel in presence of 0.3 M NaCl or more, therefore related potentiodynamic curves almost overlap with the behaviour observed in solutions not containing inhibitor (Figure 1a). On the other hand, with low concentration of chloride ions the pitting potential in the presence of DMEA increases (-0.06 V SCE) compared to that observed in absence of inhibitor (-0.25 V SCE). In presence of a higher concentration of DMEA and low concentration of chlorides the pitting potential is about 400 mV higher than the pitting potential observed in absence of inhibitor, while with 0.3 M or 1 M NaCl the inhibitive effect is lost again (Figure 1b).

Figure 2 summarises the results of potentiodynamic polarization tests on all inhibitors, in the form of pitting potential (E_{pit}) and increase in pitting potential (ΔE_{pit}), for the most relevant experimental conditions – i.e., 0.1 M solutions of the inhibitors and 0.1 M or 0.3 M NaCl; data collected in 1 M NaCl are not presented, since the performance of most inhibitors was poor and no protection was achieved. Tartrate, benzoate and glutamate all resulted in a good inhibition effect at the lower chloride concentration, with ΔE_{pit} larger than 650 mV compared to the reference solution, while amine-based inhibitors – DMEA and to a lower extent TETA – were less performing, with an

increase in E_{pit} of 190 mV and 480 mV, respectively. DMEA substances did not produce any significant inhibitive action in the solution containing 0.3 M NaCl, where E_{pit} was substantially unaltered with respect to the reference solution. Conversely, in presence of 0.3 M NaCl benzoate and glutamate allowed a small increase in E_{pit} (110 mV and 230 mV, respectively). Tartrate was the only substance to maintain a good inhibitive performance, with E_{pit} almost 500 mV higher than reference conditions.

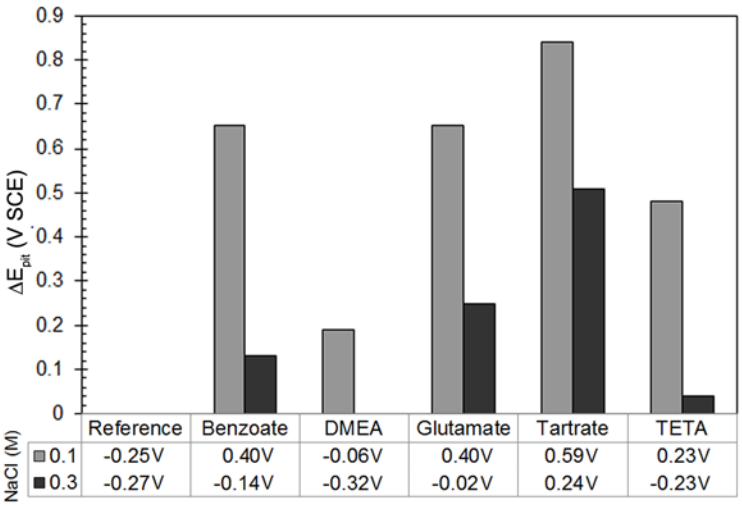

Figure 2 – Increase in pitting potential, ΔE_{pit}, in presence of different inhibitors all in concentration 0.1 M, in simulated pore solution with the addition of 0.1 M or 0.3 M NaCl. Values given in table represent pitting potential, E_{pit}, in V SCE

3.2 Free corrosion

Free corrosion tests were performed in simulated pore solution containing 0.1 M NaCl, with the addition of inhibitors in concentrations ranging from 0.001 to 0.1 M. The initiation time for chloride induced corrosion is reported in Figure 3: as a comparison, in simulated pore solution with 0.1 M NaCl and without inhibitors time-to-corrosion was 2 h. Once again, carboxylate compounds – benzoate and tartrate – were the best performing inhibitors and the time-to-pitting increased with increasing inhibitor concentration. Glutamate showed intermediate behaviour, while amines showed time-to-pitting values lower than 50 h even at the highest concentration.

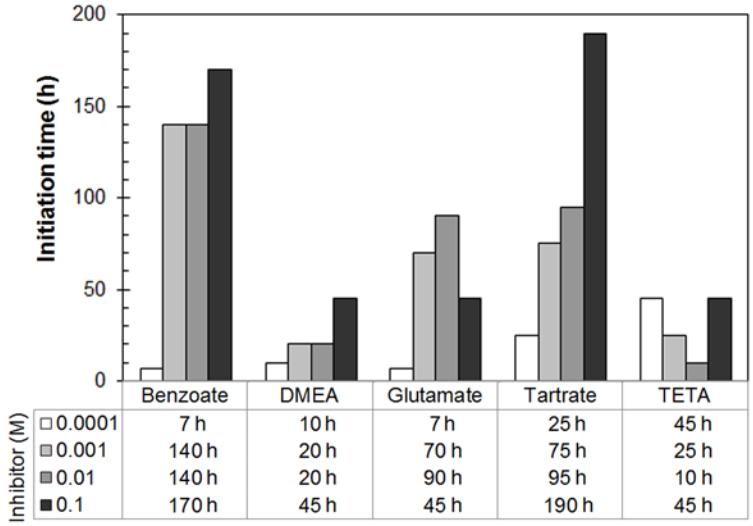

Figure 3 – Initiation time (in hours) in simulated pore solution with 0.1 M NaCl and increasing concentrations of inhibitors

3.3 Electrochemical impedance spectroscopy

Concerning EIS analyses, once more tests were performed in simulated pore solution containing increasing quantities of inhibitor, in presence or absence of chlorides. As described in the Experimental section, samples were immersed in alkaline solution, their open circuit potential was measured after 48 hours of immersion to verify their passivation, EIS was performed potentiostatically by imposing the measured E_{OCP}. Then, 0.1 M NaCl was added and EIS was repeated at fixed times until pitting corrosion occurred.

Table 2 – Open circuit potential (E_{OCP}) used as potential value in EIS measurements performed before NaCl addition, immediately after NaCl addition and at fixed times after NaCl addition; values are in mV SCE, values in bold indicate the occurrence of pitting

	No NaCl	*0.1 M NaCl*						
	48 h in SPS + inhibitor	*0 h*	*24 h*	*48 h*	*72 h*	*144 h*	*168 h*	*192 h*
Benzoate	-160	-150	-160	-150	-140	-190	**-410**	**-390**
DMEA	-150	-145	-195	**-400**	**-375**	**-390**	**-400**	**-410**
Glutamate	-210	-190	-230	-215	**-390**	**-400**	**-390**	**-405**
Tartrate	-200	-205	-190	-190	-180	-185	-180	**-380**
TETA	-180	-175	-220	**-420**	**-405**	**-400**	**-370**	**-390**

Table 2 summarises the values of E_{OCP} at which each EIS was performed in solutions containing 0.1 M inhibitors. Values in bold indicate the occurrence of pitting: it is possible to notice that this

corresponds to sole 48 h of immersion in alkaline solution with NaCl for both amine-based inhibitors, while the aminoacid allowed one more day before initiation and carboxylates reached 168 h (benzoate) and 192 h (tartrate) of resistance to pitting initiation, confirming free corrosion data.

Figure 4 reports an example of how the electrochemical impedance measurements evolved in time: benzoate is presented as sample substance, with concentration 0.1 M. No significant alteration was noticed in the shape of the curves, which overlap almost perfectly until the formation of pits occurred, after several days (Table 2): in fact, an incubation time is needed before pitting initiation on carbon steel in alkaline environment. In details, phase plots showed a capacitive response from the systems, as seen in the constant value reached at medium and low frequencies (~-80°) which suggests the filming ability of the inhibitor on the metal surface. Two overlapped time constants are observed as well, which indicate the presence of two electrochemical processes occurring simultaneously.

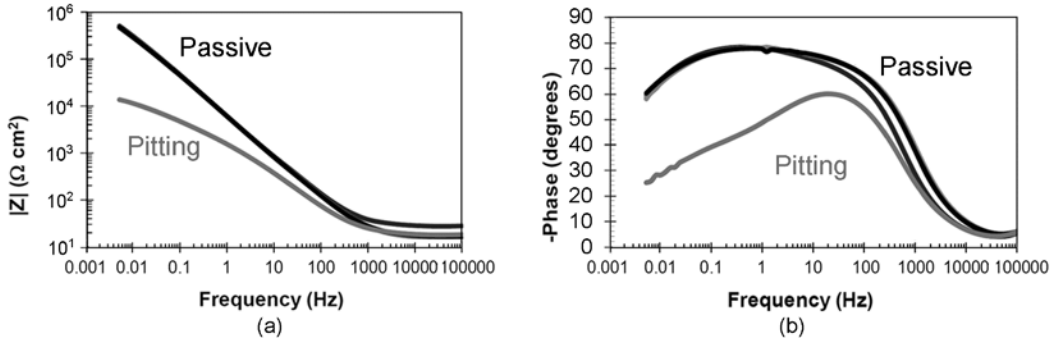

Figure 4 – Impedance modulus (a) and phase (b) in simulated pore solution containing 0.1 M benzoate: two curves representing the passive material (recorded at 0 h and 48 h after NaCl addition) and one representing pitting condition (recorded 168 h after NaCl addition) are presented

Similar trends were observed in presence of all inhibitors, together with a progressive increment in the impedance of the system with increasing inhibitor concentration, which was related to the formation of a more stable film on the surface.

The most relevant parameters describing surface interactions were extrapolated from experimental data by applying an equivalent circuit $R_s(Q_1R_1)(Q_2R_2)$. Here R_s is solution resistance, R_1 and Q_1 represent the charge transfer resistance and the double layer, where processes occur at high frequencies (fast response), while R_2 and Q_2 are resistance and capacitance of the passive layer, whose redox processes can be identified as phenomena occurring at low frequencies [11,43-45]. As a consequence of this equivalent circuit, interactions between substrate and inhibitor are described by R_1 and Q_1.

Due to presence of heterogeneities on the surface, a constant phase element Q is introduced instead of a capacitor, to allow a non-ideal response of the system [11,43-45]. Capacitance is expressed as

[$S \cdot s^n/cm^2$], where *S* is Siemens, *s* is time in seconds, and *n* is related to the non-ideal condition. If *n* is equal to 1, the double layer behaviour is close to the ideal capacitor, reflecting the homogeneity of the solid/liquid interface. In the data presented in this work, *n* is equal to 0.97, indicating an almost purely capacitive response of the double layer. In Figure 5 the evolution of R_1 and Q_1 at increasing inhibitor concentration is given. As expected, the charge transfer resistance, R_1, increased as inhibitor concentration increased, indicating a decrease in corrosion rate, with the exception of TETA and DMEA, where the variation is less pronounced, as a result of the poor inhibiting effect of the substances. On the contrary, the highest R_1 was achieved in presence of tartrate, which produced the best corrosion resistance performances. In most cases, double layer capacitance, Q_1, decreased with increasing inhibitor concentration, which proves the formation of a homogeneous film; this behaviour is less evident in the case of DMEA, whose results do not vary with concentration, which further proves the limited performance of such inhibitor in the tested conditions.

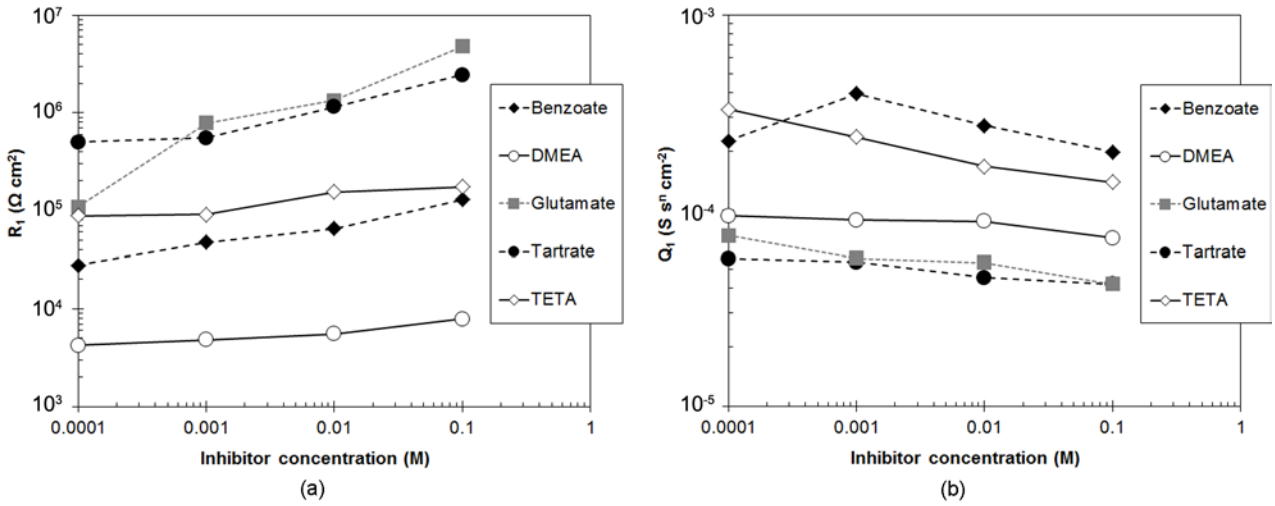

Figure 5 – Evolution of charge transfer resistance, R_1, and double layer capacitance, Q_1 with inhibitor concentration (white: amines, grey: long chain aminoacid, black: carboxylate compounds)

3.4 Adsorption isotherms

As described in section 2.2, EIS and potentiodynamic polarization results were further processed to calculate the isotherm adsorption parameters, as indicative of the adsorption behaviour of the substances tested. The Temkin isotherm and the generalised Langmuir-Freundlich (LF) isotherm were chosen. Results are reported in Table 3 and Figure 6.

While chemisorption generally requires a standard free energy of adsorption, ΔG^0_{ads}, in the order of -100 kJ/mol, some studies suggest chemisorption at lower energies of -39 kJ/mol [11, 29]. Nevertheless, results here presented suggest a weak interaction between the inhibitors and the passive film. Still, the ΔG^0_{ads} obtained for benzoate with generalised LF is very close to values

reported in literature, e.g. by Kern and Landolt, who indicated a value of -28.44 kJ/mol for benzoate adsorbed on passive iron using the generalised LF isotherm [37].

Table 3 – Fitting results for generalised Langmuir-Freundlich and Temkin isotherms for all inhibitors considered

	Generalised LF				*Temkin*			
	h	K_{ads} (L/mol)	ΔG^o_{ads} (kJ/mol)	R^2	f	K_{ads} (L/mol)	ΔG^o_{ads} (kJ/mol)	R^2
Benzoate	0.37	972	-27	0.97	12.4	4.7×10^5	-42	0.97
DMEA	0.71	16	-17	0.88	15.4	8×10^3	-32	0.97
Glutamate	0.65	9,450	-33	0.91	12	4.5×10^6	-48	0.8
Tartrate	0.6	129	-22	0.99	8.8	1.2×10^4	-33	0.95
TETA	0.18	5,800	-31	0.89	24.4	1.2×10^9	-62	0.88

The low ΔG^0_{ads} observed in some cases can be explained as an effect caused by the displacement of water molecules from the surface, since water has a high energy of adsorption for metals of the iron group and therefore it can contribute to the measured ΔG^0_{ads}, which in turn is susceptible to solvent effects. Overall, glutamate and TETA appear to present the stronger adsorption to the substrate, which contradicts potentiodynamic and impedance tests results: not only their adsorption constants are high, but their free energies are the most favourable to adsorption. Regarding the binding strength of TETA on steel surfaces, examples are reported in literature regarding both passive and active state, supporting the free energies here calculated but contradicting experimental results [46-48].

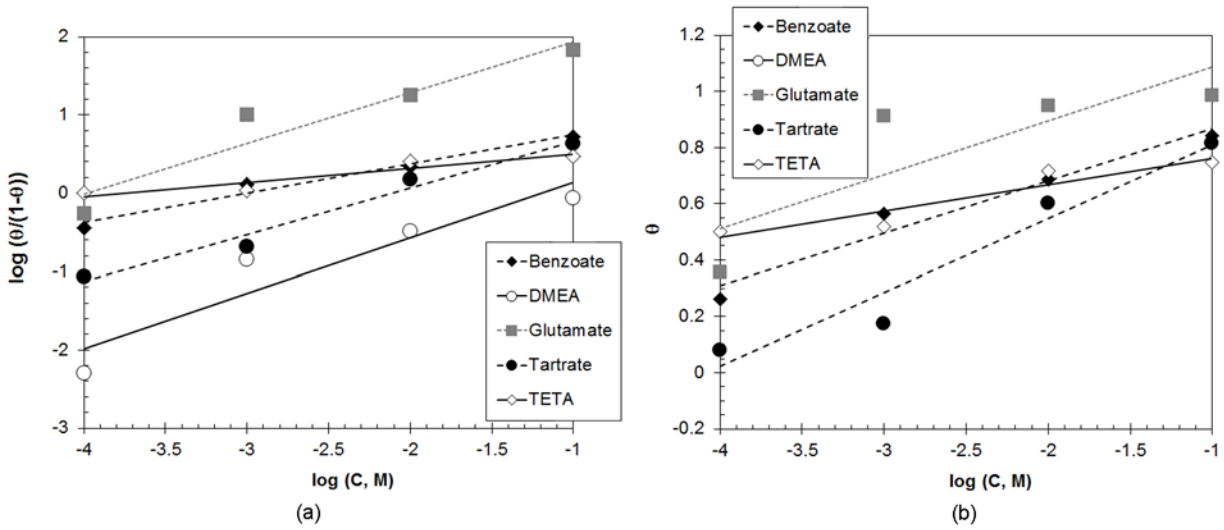

Figure 6 – a) generalised Langmuir-Freundlich isotherm and b) Temkin isotherm at increasing inhibitor concentration (white: amines, grey: long chain aminoacid, black: carboxylate compounds)

On the other hand, the processing of the two isotherms present notably different values of adsorption energy: in particular, in some cases the Temkin isotherm appears to overestimate the ΔG^0_{ads} of a given inhibitor. This may be due to the difference in their interaction factor: *h* is related to substrate heterogeneities from the adsorption point of view, whereas *f* not only indicates the presence of heterogeneities on the surface, but also the presence of lateral interaction, i.e., attraction and repulsion between adsorbed molecules. *h* values observed indicate that passive carbon steel has very irregular surface properties. Conversely, *f* values are positive and quite high, indicating surface irregularities as well as the presence of repulsive interactions between adsorbed and adsorbing molecules [37,49,50]. This difference may explain the higher ΔG^0_{ads} obtained for tartrate, in spite of its condition of best performing inhibitor.

3.5 Molecular Mechanics and Molecular Dynamics Study

3.5.1 Inhibitor molecules: the isolated molecule and its adsorption on the γ-FeOOH surface

At first the isolated inhibitor molecules were studied, followed by the single molecules near the surface of lepidocrocite (γ-FeOOH) in two different initial trial geometries, namely parallel or perpendicular to the surface. For the most stable geometry eventually obtained, the interaction energy between the inhibitor and the lepidocrocite surface – i.e., the passive carbon steel – were caoculated. This energy is defined as $E_{int} = E_{tot} - (E_{free} + E_{substr})$, where E_{tot} is the energy of the whole system, E_{free} is the energy of the free inhibitor molecule, and E_{substr} is the energy of the lepidocrocite surface (in this case, it is a constant conveniently set to zero since all the surface atoms are kept fixed). This energy represents the energy gain shown by the system upon adsorption of the inhibitor molecule on the surface from its free state. In particular a lower E_{int} implies a stronger adsorption. The calculated values of the interaction energy for all the inhibitors considered in this paper are reported in Figure 7.

<Figure 7>

It is also of interest to note for the later discussion that isolated benzoate and glutamate form one hydrogen bond with the surface between the carboxylate anion and the hydrogen of γ-FeOOH, while tartrate forms a similar bidentate hydrogen bond of one carboxylate with two neighbouring hydrogens of the surface and a further one involving a tartrate hydroxyl and a surface oxygen atom. On the other hand, in this stage DMEA and TETA (and more generally amine groups) do not form

any hydrogen bond with the surface. By comparing the resulting adsorption energies, it is possible to establish a preliminary adsorption ranking for the studied substances, where tartrate and glutamate show the strongest adsorption, and DMEA the weakest one.

3.5.2 Monolayers of inhibitor molecules

In order to investigate how the inhibitor molecules interact among themselves and with the substrate, assemblies of 16, 25 and 36 molecules were initially placed both in an ordered arrangement and in a random one near the surface. However, afterwards only the larger sample of 36 molecules initially distributed randomly near the surface was considered, as the best one to study the partial or total surface coverage, as obtained after the MD runs.

Figure 8 shows the arrangement of 36 inhibitor molecules after the initial energy minimization carried out with periodic boundary conditions, starting from a random distribution near the surface.

<Figure 8>

As previously observed, by starting with an initially ordered arrangement of the inhibitor layer, a simple energy minimization already induced some local disorder with a slightly more compact arrangement, in some cases, independently of the surface density of molecules. It was now found that starting with an already disordered, random arrangement of the inhibitor molecules close to the surface the initial optimization provides some well-defined aggregates and a surface that is not fully covered, thus exposing the underlying substrate (Figure 8).

The change in molecular positions is due to intermolecular interactions, either attractive or repulsive, in the presence of attractive interactions with the surface. In fact, the (delocalised) negative charges on the carboxylate groups of different molecules, when present, can result in repulsive forces which make them drift apart. Conversely, the presence of hydroxyl or amino groups that can form hydrogen bonds with the carboxylate (if present) or with the same groups in adjacent molecules may produce attractive intermolecular interactions. This is more apparent in the case of DMEA and tartrate, whereas no such effect is clearly present with the other inhibitors.

MD calculations were then performed to monitor the time evolution and the possible rearrangement of the layer of adsorbed molecules. Figure 9 shows the final snapshots of the conformations obtained starting from the optimised ones presented in Figure 8. These simulations were again carried out with implicit solvent and periodic boundary conditions. In general, MD runs led to an even surface covering with the formation of a monolayer of inhibitor molecules, or a thicker layer in the case of TETA due to the larger molecular size. In this case, the interaction energy E_{int} per molecule due both to the surface adsorption and to the close contacts with the neighbouring

molecules was obtained by first dividing the total energy of the system by the number of adsorbed molecules, and then proceeding as before. The resulting values are also reported in Figure 9.

<Figure 9>

Considering both geometrical features shown by Figure 9 and quantitative information obtained from the pair distribution function PDF, it is important to consider the main geometrical and energetic factors affecting the coverage of the γ-FeOOH surface.

In the case of benzoate, the inhibitor molecules assume both a perpendicular and a parallel arrangement in order to optimize at the same time the surface and the intermolecular interactions. In either case, benzoates largely form the above-mentioned hydrogen bonds involving carboxylate anion and surface hydroxyl, while still experiencing repulsive intermolecular electrostatic interactions. Therefore, the adsorbed monolayer exposes to the outer environment the aromatic rings parallel or perpendicular to the surface, but also the carboxylate groups, as clearly seen in Figure 9.

With glutamate, surface interactions take place again through hydrogen bonds, involving one carboxylate anion and surface hydroxyls, but also the amino group through an N-H···O hydrogen bond. Moreover, inhibitor molecules do also form intermolecular hydrogen bonds involving the COO^- and the NH_2 groups. A fraction of the carboxylate oxygens are therefore buried and in contact with the surface, but a significant fraction of them is exposed together with part of the amino groups (Figure 9). Tartrate shows also a large number of hydrogen bonds between carboxylate anions and surface hydroxyls, but again a significant fraction of carboxylate is found far from the surface together with some hydroxyl groups, while also in this case the inhibitor molecules form many intermolecular hydrogen bonds.

On the other hand, DMEA forms several hydrogen bonds between its hydroxyl hydrogens and the surface oxygen atoms, but very few, if any, intermolecular hydrogen bonds. Finally, TETA can form many hydrogen bonds with the surface through the amine hydrogens and the surface oxygens, but only some intermolecular hydrogen bonds. It should be noted here that the thick layer created by TETA is not a real double layer, because several molecules span the whole film height, and only a few of them are entirely sitting above the first layer of adsorbed atoms. Accordingly, the average interaction energy reported in Figure 9 is due to the surface interaction of the adsorbed molecules, but also to the interactions of the upper molecules with the lower ones, thus enhancing the apparent stability of the adsorbed film. Finally, DMEA TETA do not carry any net charge, and therefore they do not experience major electrostatic repulsive interactions among the adsorbed molecules.

The average atom distribution above the surface of the adsorbed inhibitors is best discussed through the pair distribution function PDF (see paragraph 2.3). The calculated PDF gives here the probability density of finding a given group of inhibitor atoms at a distance between r and r+dr from the exposed surface atoms. The most relevant PDFs are shown in Figure 10.

<Figure 10>

In the left panel of Figure 10, the first sharp peak at $r \approx 2.7 - 2.8$ Å is due to the carboxylate oxygens or to some tartrate hydroxyls close to, and hydrogen bonded to, the surface OH. Interestingly, after this peak a plateau is observed for tartrate and glutamate, extending up to about 6.3 Å, where a small peak is present corresponding to the carboxylate oxygens at this distance from the surface and protruding outwards. Conversely, the tartrate hydroxyls are mostly found either close to the surface, as just said, but also exposed to the outer environment, being close to – though still below – the upper film profile at 5.1 Å from the surface, as shown by their second peak (uppermost curve in the left panel of Figure 10). No further peak beyond the first one is found for benzoate at larger r, but rather a poorly defined shoulder produced by the COO^- being parallel or perpendicular to the surface. Such arrangement leads also to a different distribution of the benzoate hydrogens, which are found at roughly 3.5 Å from the surface in the parallel arrangement, and at distances ranging from 2.8 Å to 6.0 Å in the perpendicular arrangement (see Figure S1 of Supplementary Information), thus possibly contributing to the benzoate inhibitor activity by forming a steric barrier to chlorides. It should also be noted that in glutamate the amino N atoms are found either relatively close to the surface at a distance of about 3 Å, or within the adsorbed film at about 5.3 Å from the surface (see the snapshot in Figure 9 and the PDF in Figure S2 of Supplementary Information). Interestingly, in neutral inhibitors only DMEA can approach the surface through its hydroxyls hydrogen-bonded to the surface OH at distances of 2.6 Å, corresponding to the first small peak of the PDF, and of 2.9 Å, where the tallest peak is found in the right panel of Figure 10. DMEA hydroxyls are however also scattered in the film at varying distances from the surface up to a distance indicated by the peak at about 6.2 Å from the surface, while the N atoms of the amino groups are broadly distributed at an average distance of about 4 Å from the surface. Conversely, in TETA only a small peak is found close to the surface, indicating that the majority of the amino groups are distributed within the whole thickness of the adsorbed film.

4. Discussion

Considering the potential inhibition mechanisms involved, a first, crucial consideration is that inhibitor molecules must include an available electron pair to enhance the molecule adsorption on the passive film: this requirement is complied with by both amine and carboxylate based inhibitors. Moreover, surface coverage must be as complete as possible: this should also take into account competitive adsorption of polar molecules or charged ions present in solution, such as water and chloride ions, which can occupy potential adsorption sites and even detach the inhibitor molecules. Therefore, an ideal inhibitor should adsorb strongly and cover the whole surface.

Candidate inhibitors may display only one of the aforementioned properties, such as a relatively high adsorption strength but in the presence of large intermolecular interactions leading to strong clustering, they might leave surface patches exposed to the corrosive environment at low concentration. Alternatively, molecules with a lower adsorption strength yielding a good surface coverage and exposing carboxylate moieties (or other anionic groups) may produce significant inhibition effects through electrostatic repulsion of chloride ions. The resulting pitting potential is high, in agreements with previous findings [25].

Electrochemical tests have the important feature to give the final behaviour as a result of the combination of the two above-discussed requirements. From such tests tartrate, glutamate and benzoate were identified as the molecules inducing the highest increase in pitting potential, i.e., providing the best resistance to chloride-induced corrosion (Figure 2). The inhibitive effect of tartrate and benzoate was also confirmed by the highest time-to-corrosion recorded (Figure 3). Moreover, glutamate and tartrate showed the highest charge transfer resistance (R_1), i.e., the lowest corrosion rate, as well as the lowest double layer capacitance (Q_1), i.e., the highest homogeneity of the adsorbed organic layer (Figure 5). The intermediate values of benzoate, both in terms of adsorption energy (Figure 8) and of electrochemical behaviour (Figure 5), confirm its limited protectiveness, and can be ascribed to the presence of a single carboxylic group, compared with the more efficient tartrate which contains two carboxylic groups.

MD simulations yielded a quantitative picture of the surface arrangements of molecules in the adsorbed layer. While surface coverage is essentially complete in all cases due to the large surface concentration assumed in the simulations, it is possible to relate the inhibitor activity shown in particular by the anionic ones to the repulsive electrostatic interaction between chloride anions and exposed carboxylates, clearly shown by MD simulations (Figure 10). Clearly such repulsions would be absent in the amino-based inhibitors and in the presence of amino groups, which conversely could protect to some extent the surface by purely steric effects (which incidentally would also be present in the other inhibitors), but which may favour the surface proximity of chloride anions through their NH_2 groups due to possible ion-dipole interactions, so that Cl^- could approach the positive side of the $^{\delta+}H–N^{\delta-}$ bond. A similar consideration applies to the interaction between Cl^-

and OH groups, which therefore would decrease somewhat the inhibiting behavior outlined before in glutamate and tartrate, but obviously not in benzoate where no hydroxyl groups are present. On the other hand, the potential complexation ability of the amino and hydroxyl groups towards the cations largely present in concrete (mainly, though not only, Ca^{2+}) would complicate the above theoretical picture. Such issues could be tackled by further more realistic, but also much more demanding simulations that are currently being planned.

5. Conclusions

On the basis of the correlation of experimental data and molecular modelling, the efficiencies of different corrosion inhibitors in protecting carbon steel from corrosion in concrete were compared. Tartrate presented the best inhibitive behaviour on account of its adsorption strength, excellent surface coverage and the repulsive effect exerted on chlorides by the exposed carboxylate anions. Benzoate also showed a favourable adsorption energy and a uniform distribution when adsorbing on γ-FeOOH, which is crucial to produce efficient inhibition. Moreover, glutamate showed the strongest calculated adsorption among the anionic inhibitors, with a carboxylate distribution similar to tartrate, factors which allowed reaching a high pitting potential. Finally, amines show poor inhibition effect because of a poor repulsive interaction with chloride ions, confirming the experimental evidence of this work as well as of previous ones.

More generally, it is possible to confirm the favourable interaction energy between the γ-FeOOH surface and the adsorbed molecules, with the onset of repulsive intermolecular interactions among anions. Based on these observations, molecular mechanics and molecular dynamics confirm to be an additional, powerful tool to understand the behaviour of inhibitors in the presence of a bare or passivated metallic surface, as well as to predict their potential efficiency in inhibiting steel corrosion in the chosen environmental conditions.

References

[1] L. Bertolini, B. Elsener, E. Redaelli, P. Pedeferri, R. Polder, Corrosion of steel in concrete: prevention, diagnosis, repair, 2nd ed., Wiley: Weinheim, 2013.

[2] B. Elsener, Corrosion inhibitors for steel in concrete - State of the art report, EFC Publications, Number 35, Institute of Material: London, 2001.

[3] N.S. Berke, Nitrite-base corrosion inhibitors for reinforced concrete, Mater. Perform. 28 (1989) 41-48.

[4] N.S. Berke, T.G. Weil, World-wide review of corrosion inhibitors in concrete; advances in concrete technology, Int. Conf. CANMET, Athens, Greece, 1992, 899-924.

[5] C. Andrade, C. Alonso, J.A. Gonzalez, Cement, Concrete and Aggregates 8 (1986) 110-116.
[6] C. Monticelli, A. Frignani and G. Trabanelli, A study on corrosion inhibitors for concrete application, Cem. Concrete Res. 30 (2000) 635-642.
[7] C. Andrade, C. Alonso, M. Acha, B. Malric, Na_2PO_4F as inhibitor of corroding reinforcement in carbonated concrete, Cem. Concrete Res. 26 (1996) 405-415.
[8] V.T. Ngala, C.L. Page, M.M. Page, Corrosion inhibitor system for remedial treatment of reinforced concrete. Part 2: sodium monofluoroposphate, Corros. Sci. 45 (2003) 1523-1537.
[9] C.K. Nmai, S.A. Farrington, G.S. Bobrowsky, Organic based corrosion inhibiting admixtures for reinforced concrete, Concrete Int. 14 (1992) 45-51.
[10] U. Mäder, A new class of corrosion inhibitors for reinforced concrete, Concrete 9 (1999) 215-232.
[11] H.E. Jamil, M.F. Montemor, R. Boulif, A. Shriri, M.G.S. Ferreira, An electrochemical and analytical approach to the inhibition mechanism of an amino-alcohol-based corrosion inhibitor for reinforced concrete, Electrochim. Acta 48 (2003) 3509-3518.
[12] J.M. Gaidis, Chemistry of corrosion inhibitors, Cem. Concrete Compos. 26 (2004) 181-189.
[13] M. Ormellese, M. Berra, F. Bolzoni, T. Pastore, Corrosion inhibitors for chlorides induced corrosion in reinforced concrete structures, Cem Concrete Res. 36 (2006) 536-547.
[14] F. Bolzoni, S. Goidanich, L. Lazzari, M. Ormellese, Corrosion inhibitors in reinforced concrete structures. Part 2. Repair system, Corros. Eng. Sci. Technol. 41 (2006) 212-220.
[15] L. Mechmeche, L. Dhouibi, M. Ben Ouezdou, E. Triki, F. Zucchi, Investigation of the early effectiveness of an amino-alcohol based corrosion inhibitor using simulated pore solutions and mortar specimens, Cem. Concrete Compos. 29 (2007) 365-372.
[16] T.A. Söylev, M.G. Richardson, Corrosion inhibitors for steel in concrete: State-of-the-art report, Constr. Build. Mater. 22 (2008) 609-622.
[17] X. Zhou, H. Yang, F. Wang, Investigation on the inhibition behaviour of a pentaerythritol glycoside for carbon steel in 3.5% NaCl saturated $Ca(OH)_2$ solution, Corros. Sci. 54 (2012) 193-200.
[18] M. Criado, C. Monticelli, S. Fajardo, D. Gelli, V. Grassi, J.M. Bastidas, Organic corrosion inhibitor mixtures for reinforcing steel embedded in carbonated alkali-activated fly ash mortar, Constr. Build. Mater. 35 (2012) 30-37.
[19] E. Rakanta, Th. Zafeiropoulou, G. Batis, Corrosion protection of steel with DMEA-based organic, Constr. Build. Mater. 44 (2013) 507-513.
[20] E. Rakanta1, T. Zafeiropoulou, G. Batis, Corrosion protection of steel with DMEA-based organic inhibitor, Constr. Build. Mat, 44 (2013) 507–513

[21] F-L. Fei, Jie Hu, J-X. Wei, Q-J. Yu, Z-S. Chen, Corrosion performance of steel reinforcement in simulated concrete pore solutions in the presence of imidazoline quaternary ammonium salt corrosion inhibitor, Constr. Build. Mater. 70 (2014) 43-53.
[22] S.M. Abd El Haleem, S. Abd El Wanees, A. Bahgat, Environmental factors affecting the corrosion behaviour of reinforcing steel. VI. Benzotriazole and its derivates as corrosion inhibitors of steel, Corros. Sci. 87 (2014) 321-333.
[23] L. Feng, H. Yang, F. Wang, Experimental and theoretical studies for corrosion inhibition of carbon steel by imidazoline derivative in 5% NaCl saturated Ca(OH)2 solution, Electrochim. Acta 58 (2011) 427-436.
[24] J. Hu, D.A. Koleva, P. Petrov, K. Van Breugel, Polymeric vesicles for corrosion control in reinforced mortar: electrochemical behaviour, steel surface analysis and bulk matrix properties, Corros. Sci. 65 (2012) 414-430.
[25] M. Ormellese, L. Lazzari, S. Goidanich, G. Fumagalli, A. Brenna, A study on organic substances as inhibitors for chloride-induced corrosion in concrete, Corros. Sci. 51 (2009) 2959-2968.
[26] L. Yohai, M. Vázquez, M.B. Valcarce, Phosphate ions as corrosion inhibitors for reinforcement steel in chloride-rich environments, Electrochim. Acta, 102 (2013) 88–96.
[27] F. Fei, J. Hu, J.-X. Wei, Q-J Yu, Z-S Chen, Corrosion performance of steel reinforcement in simulated concrete pore solutions in the presence of imidazoline quaternary ammonium salt corrosion inhibitor, Constr. Build. Mat, 70 (2014) 43–53
[28] X. Zhou, H. Yang, F. Wang, Investigation on the inhibition behavior of a pentaerythritol glycoside for carbon steel in 3.5% NaCl saturated $Ca(OH)_2$ solution, Corros. Sci., 54 (2012) 193-200
[29] L. Valek, S. Martinez, D. Mikulić, I. Brnardić, The inhibition activity of ascorbic acid towards corrosion of steel in alkaline media containing chloride ions, Corros. Sci., 50 (2008) 2705-2709
[30] A. Kokalj, Molecular modelling of organic corrosion inhibitors: why bare metal cations and not appropriate models of oxidized metal surfaces and solvated metal cations, Acta Chim. Slov. 61 (2014) 340-349.
[31] J.K. Singh, D.D.N. Singh, The nature of rusts and corrosion characteristics of low alloy and plain carbon steels in three kinds of concrete pore solution with salinity and different pH, Corros. Sci. 56 (2012) 129-142.
[32] P. Ghods, O.B. Isgor, G.J.C. Carpenter, J. Li, G.A. McRae, G.P. Gu, Nano-scale study of passive films and chloride-induced depassivation of carbon steel rebar in simulated concrete pore solutions using FIB/TEM. Cem. Concrete Res. 47(2013) 55-68.

[33] L. Freire, X.R. Nóvoa, M.F. Montemor, M.J. Carmezim, Study of passive films formed on mild steel in alkaline media by the application of anodic potentials. Mater. Chem. Phys. 114 (2009) 962-972.
[34] P. Ghods, O. Burkan Isgor, F. Bensebaa, D. Kingston, Angle-resolved XPS study of carbon steel passivity and chloride-induced depassivation in simulated concrete pore solution, Corros. Sci. 28 (2012) 159-167.
[35] Materials Studio distributed by *Accelrys Inc*., San Diego, CA. See http://www.accelrys.com.
[36] P. Kern, D. Landolt, Adsorption of an Organic Corrosion Inhibitor on Iron and Gold Studied with a Rotating EQCM. J. Electrochem. Soc. 148 (2001) B226-B235.
[37] P. Kern, D. Landolt, Adsorption of organic corrosion inhibitors on iron in the active and passive state. A replacement reaction between inhibitor and water studied with the rotating quartz crystal microbalance. Electrochim. Acta 47 (2001) 589-598.
[38] Z.V.P. Murthy, K. Vijayaragavan, Mild steel corrosion inhibition by acid extract of leaves of Hibiscus sabdariffa as a green corrosion inhibitor and sorption behavior. Green Chem. Lett. Rev. 7 (2014) 209-219.
[39] H.W. Tian, W.H. Li, D.P. Wang, B.R. Hou, Adsorption Mechanism of Nicotinic Acid onto a Passive Iron Surface. Acta Phys. Chim. Sin. 28 (2012) 137-145.
[40] F. Ganazzoli, G. Raffaini, Computer simulation of polypeptide adsorption on model biomaterials, Phys. Chem. Chem. Phys. 7 (2005) 3651-3663.
[41] G. Raffaini, L. Melone, C. Punta, Understanding the topography effects on competitive adsorption on a nanosized anatase crystal: A molecular dynamics study, Chem. Commun. 49 (2013) 7581-7583.
[42] H. Sun, COMPASS: An ab Initio Force-Field Optimized for Condensed-Phase Applications Overview with Details on Alkane and Benzene Compounds. J. Phys. Chem. B 102 (1998) 7338-7364.
[43] C. Andrade, M. Keddam, X.R. Nóvoa, M.C. Pérez, C.M. Rangel, H. Takenouti, Electrochim. Acta 46 (2001) 3905-3912.
[44] S. Joiret, M. Keddam, X.R. Nóvoa, M.C. Pérez, C. Rangel, H. Takenouti, Cem. Concrete Compos. 24 (2002) 7-15.
[45] Q. Yin, G. H. Kelsall, D. J. Vaughan, and N. P. Brandon, Journal of The Electrochemical Society, 148 (2001) A200-A208.
[46] M.J. Incorvia, S. Contarini**,** X-Ray Photoelectron Spectroscopic Studies of Metal/Inhibitor Systems: Structure and Bonding at the Iron/Amine Interface, J. Electrochem. Soc. 136 (1989) 2493-2498.

[47] S. Sathiyanarayanan, C. Marikkannu, N. Palaniswamy, Corrosion Inhibition Effect of Tetramines for Mild Steel in 1M HCl, Appl. Surf. Sci. 241 (2005) 477-484.
[48] B. Bozzini, C. Mele, and V. Romanello, An in situ FT-IR evaluation of candidate organic corrosion inhibitors for carbon steel in contact with alkaline aqueous solutions, Mater. Corros. 58 (2005) 362-368.
[49] W. Durnie, R. De Marco, A. Jefferson, B. Kinsella, Development of a Structure-Activity Relationship for Oil Field Corrosion Inhibitors, J. Electrochem. Soc. 146 (1999) 1751-1756.
[50] E. Gileadi, Electrode Kinetics for Chemists, Chemical Engineers and Material Scientists, Wiley-VCH, Inc.: New York, 1993.